Applied Thermal Engineering 126 (2017) 1126–1133

Contents lists available at ScienceDirect

Applied Thermal Engineering

journal homepage: www.elsevier.com/locate/apthermeng

Research Paper

Modelling and experimental investigation of a thermally driven self-oscillating pump

Marijn P. Zwier [a], Henk Jan van Gerner [b], Wessel W. Wits [a,*]

[a] Faculty of Engineering Technology, University of Twente, P.O. Box 217, 7500 AE Enschede, The Netherlands
[b] Thermal Control Group, Space Division, Netherlands Aerospace Centre, 8316 PR Marknesse, The Netherlands

HIGHLIGHTS

- A thermally driven self-oscillating pump is presented.
- Experimental analyses to characterize the pump were performed.
- Modelling is based on a non-linear system of coupled differential equations.
- The maximum pump flow rate is 0.0013 kg/s and a 0.25 bar pressure head.
- The thermally driven pump has good potential for aerospace applications.

ARTICLE INFO

Article history:
Received 5 September 2016
Revised 18 January 2017
Accepted 15 February 2017
Available online 16 February 2017

Keywords:
Two-phase oscillating flow
Oscillating meniscus
Pulsating heat pipe
Pump efficiency
Pumping characteristics

ABSTRACT

This paper explores the pumping characteristics and behaviour of a thermally driven self-oscillating pump. The pump consists of a single wickless capillary tube with a circular cross-section. The tube is closed at one end and has a T-section with two check valves at the other end to provide for a one directional flow. An experimental setup was built to investigate the output mass flow and pressure head of the pump. During the experiments, the performance of the check valves had a negative influence on the output mass flow. To determine this influence, a video analysis of the fluid oscillation without the check valves was conducted and compared to results with check valves. The average output mass flow with valves was approximately 0.0010 kg/s with a maximum measured pump flow of 0.0013 kg/s. The maximum pressure head delivered was 0.25 bar. A numerical model of the vapour bubble oscillation was developed to get a better understanding of the pump and its working principles. The model is based on the conservation of mass, momentum and energy, and resulted in a non-linear system of coupled differential equations. Overall, the experiments conducted with the thermally driven self-oscillating pump have shown that the pump has good potential to be used in aerospace applications.

1. Introduction

Thermally driven self-oscillating pumps are simple and robust pumps with a minimum of moving components that operate based on the two-phase oscillation principle of a Pulsating Heat Pipe (PHP). The self-oscillating pump of this study consists of a single wickless capillary tube with a circular cross-section. The tube is closed at one end and has a T-section with two check valves on the other end. The tube is filled with working fluid and is divided into an evaporator, adiabatic and condenser section in analogy with conventional heat pipe terminology. It should be noticed that this terminology is not entirely correct, since condensation may also occur in the evaporator, as shown by Rao et al. [1,2]. An expanding and contracting vapour bubble oscillates between the evaporator and condenser, driven by thermal energy. The vapour bubble acts like a piston, pumping fluid with the aid of the check valves.

The simplicity and robustness of the pump makes it a promising pump for space applications. The current thermal design solutions, such as heat pipes and PHP, are not always able to dissipate heat from many distributed payloads over large distances. Mechanically driven loops overcome this problem, but the sensitivity to wear makes the mechanical pumps in these loops a single point of failure. This paper explores the pumping characteristics and behaviour of a thermally driven self-oscillating pump, as a potential replacement for the mechanical pump in aerospace applications.

* Corresponding author.
E-mail address: w.w.wits@utwente.nl (W.W. Wits).

http://dx.doi.org/10.1016/j.applthermaleng.2017.02.063
1359-4311/

Nomenclature

A	area (m^2)
d	diameter (m)
g	gravity (9.81 m/s^2)
H_{fg}	latent heat of vaporization (J/kg)
L	length (m)
m	mass (kg)
p	pressure (Pa)
p_r	ambient pressure (Pa)
Re	Reynolds number
T	temperature (°C)
t	time (s)
U	heat transfer coefficient (W/m °C)
u	velocity (m/s)
x	position (m)
x_q	vapour quality

Greek letters

θ	contact angle (°)
μ	viscosity (Pa s)
ρ	density (kg/m^3)
σ	surface tension (N/m)

Subscripts

a	adiabatic
c	condenser
d	dead end
e	evaporator
l	liquid
m	meniscus
sat	saturation
t	total
v	vapour

1.1. Pumping principle

The pumping principle of the self-oscillating pump corresponds to the Open Oscillatory Heat Pipe Water Pump (OOHPWP) as constructed by Dobson [3] and is explained according to recent work of Rao et al. [1,2].

The pump working principle is as follows. At the start of each pumping cycle the tube is filled with fluid. The fluid in the evaporator section is heated to the saturation temperature, forming vapour. The ongoing evaporation of fluid, increases the vapour pressure above the ambient pressure. Therefore the meniscus at the liquid-vapour interface starts to move towards the condenser section of the tube (Fig 1a I). The fluid in front of this meniscus is pushed ahead, through the discharge valve. Thereby creating an output mass flow. As discussed by Rao et al., at the start of the meniscus motion, a thin liquid film is deposited on the tube wall behind the meniscus. This thin liquid film is responsible for the major part of the heat and mass exchange, and is the driving force of the pumping motion.

The vapour pressure reaches a maximum just before the meniscus enters the condenser, due to the still evaporating thin liquid film, and the momentum of the liquid plug. The meniscus keeps moving into the condenser (II), despite the decrease of vapour pressure. The vapour pressure decreases due to the expansion and condensation of the vapour bubble. Before the meniscus reaches its topmost position in the condenser, the vapour pressure drops below ambient pressure. This pressure decrease closes the discharge valve and opens the supply valve at almost the same time. Therefore, the last beneficial part of the meniscus stroke towards the topmost position is not used to generate output mass flow. This was observed during the experiments, liquid was forced against the flow, passing through the opened supply valve.

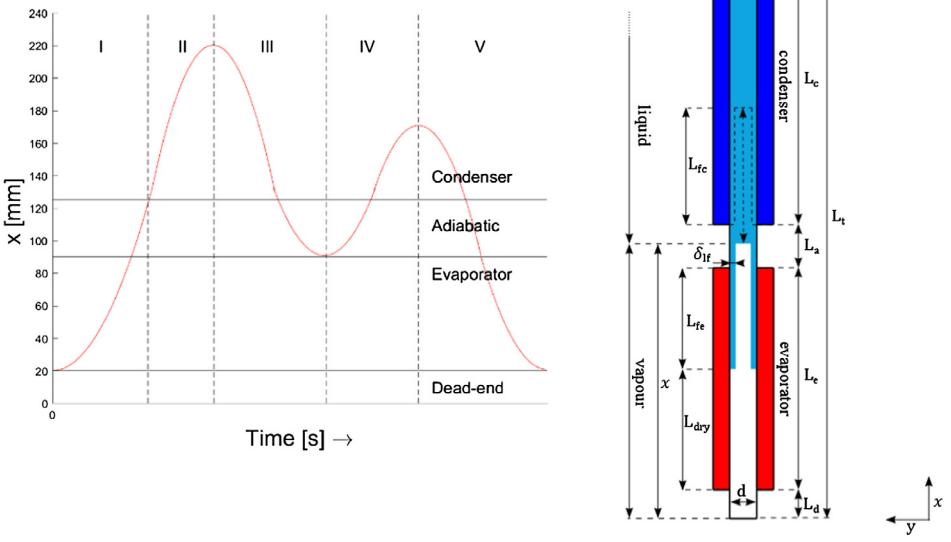

(a) the meniscus position during one cycle

(b) the geometry of the self-oscillating pump model

Fig. 1. Working principle of a self-oscillating pump.

When the meniscus returns towards the evaporator (III), the vapour pressure starts to rise again and new fluid flows through the supply valve into the tube, filling the space that was occupied by the expelled fluid and the condensed vapour bubble. Before the meniscus reaches the evaporator, the vapour pressure exceeds the ambient pressure, opening the discharge valve and closing the supply valve. Some expelled fluid will flow back into the tube as result of the open discharge valve and the meniscus movement towards the evaporator. The increase in pressure and the still present thin liquid film in the evaporator prevent the meniscus from entering the evaporator at this point in the cycle. The meniscus moves back into the condenser (IV) and again fluid is pushed out by the vapour bubble, generating output mass flow. Simultaneously the vapour pressure drops, closing the discharge valve and opening the supply valve, thus stopping the pumping motion. For the second time, the meniscus reaches the topmost position in the condenser. The thickness of the liquid film in the evaporator is reduced considerably due to the continuous evaporation and eventually fully evaporates. Because condensation is now the only tribute to the variation of the vapour mass, the pressure of the vapour bubble further decreases, pulling the meniscus back towards its starting position in the evaporator (V). This describes one cycle, that repeats itself as long as external heating and cooling is provided [1,2,4–6], resulting in the self-oscillating thermally driven pump motion.

2. Numerical model

This section presents the numerical model of the two-phase self-oscillating plug in a pump assuming ideal check valves. The equations of the model are similar to the model of Dobson and Das et al. [4,5]. Modifications and improvements are introduced in this paper to take the geometry of the pump (see Fig. 1b) into account. The model is based on the conservation of mass, momentum and energy. For all three conservations, the model is divided into three moving control volumes. The volumes represent the thin liquid film, the vapour bubble and the fluid plug.

2.1. Conservation of mass

The evaporation or mass exchange of the thin liquid film is the driving force behind the oscillation. The mass flow rate of the thin liquid film depends on the rate of evaporation, condensation and the liquid deposited on the tube wall by the moving plug. This mass flow rate can be converted into a film length inside the evaporator, assuming that evaporation only occurs in the evaporator. The length of the film (L_{lf}) is a function of the time rate of change of the film length, defined as:

$$\frac{dL_{lf}}{dt} = \begin{cases} 0 & \text{if } L_{lf} = 0, u < 0 \\ & \text{and } x \leqslant L_e + L_d \\ -\frac{\dot{m}_e}{\rho_l \pi d \delta_{lf}} & \text{if } x > L_e + L_d \\ u - \frac{\dot{m}_e}{\rho_l \pi d \delta_{lf}} & \text{otherwise} \end{cases} \quad (1)$$

The initial film thickness (δ_{lf}) is determined using a correlation developed by Han and Shikazono [7]. The mass flow rate of evaporation ($\dot{m}_e$), with the average liquid film temperature assumed equal to the saturation temperature is:

$$\dot{m}_e = \frac{U_e \pi d L_{lf}}{H_{fg_e}} (T_e - T_{sat}(p_v)) \quad (2)$$

where the heat flux crossing the film is considered conductive and the convection heat flux is neglected because the film thickness is too thin to favour viscous flow. The mass flow rate of the vapour bubble ($\dot{m}_v$) is the balance between the mass flow rate of evaporation and condensation and is described as:

$$\frac{dm_v}{dt} = \dot{m}_e + \dot{m}_{me} - \dot{m}_c - \dot{m}_{mc} - \dot{m}_{ec} \quad (3)$$

where the mass flow rate of condensation ($\dot{m}_c$), assuming that the condensed vapour is absorbed by the moving liquid plug, is defined as:

$$\dot{m}_c = \frac{U_c \pi d L_c}{H_{fg_c}} (T_{sat}(p_v) - T_c) \quad (4)$$

The final three terms in Eq. (3) are modelled similar to the mass flow rates of evaporation and condensation. $\dot{m}_{me}$ and $\dot{m}_{mc}$ are the mass flow rates of evaporation and condensation at the meniscus curvature, respectively. The final term, $\dot{m}_{ec}$ is added because the temperature of the vapourT_v may rise above the wall temperatureT_e due to the compression of the vapour bubble by the liquid plug as it returns to the evaporator section. This causes the vapour to condense onto the dry evaporator wall.

2.2. Conservation of momentum

The conservation of momentum regards the forces acting on the fluid plug. The momentum of the vapour bubble and thin liquid film are both negligible due to the low mass and the lack of viscous flow, respectively. The momentum of the fluid plug is modelled as:

$$\frac{d(m_l u)}{dt} = F_p + F_\sigma - F_g \pm F_\tau \quad (5)$$

where F_p, F_σ, F_g and F_τ are the pressure force, the capillary force, the gravitational force and the friction force, respectively. The sign of the friction force is contrary to the direction of the plug. The pressure force is:

$$F_p = A(p_v - p_r) \quad (6)$$

The capillary force is the force due to capillary action, the direction of the capillary force depends on the contact angle, tangent to the liquid surface and the tube wall. The capillary force is given by:

$$F_\sigma = \pi d \sigma \cos(\theta) \quad (7)$$

The gravitational force is given by:

$$F_g = m_l g \text{ with } m_l = (L_t - x) A \rho_l \quad (8)$$

The amount of friction depends on the friction factor C_f. Most models [4–6] use a friction factor for single-phase constant velocity flow in tubes to calculate the friction force. According to Das et al. [4] this assumption gives an underestimation of the friction force. The existence of two-phase flow during the oscillations may lead to a drastic increase of the friction force especially in the vicinity of the junction of the liquid plug with the liquid film or dry wall. In this paper the friction force is modelled using the Chisholm [8] correlation in combination with the Lockhart-Martinelli [9] parameter to determine the two-phase multiplier (Φ) that is used to correct the single-phase friction factor for two-phase flow. The Chisholm correlation with the Lockhart-Martinelli parameter (X) is defined as:

$$\Phi_l^2 = 1 + \frac{C}{X} + \frac{1}{X^2} \quad (9)$$

$$X = \left(\frac{1 - x_q}{x_q}\right)^{0.9} \left(\frac{\rho_v}{\rho_l}\right)^{0.5} \left(\frac{\mu_l}{\mu_v}\right)^{0.1} \quad (10)$$

where the value of C depends on the type of flow of the vapour and liquid. The single-phase friction factor depends on the Reynolds number of the liquid and is defined as:

$$C_f = \begin{cases} 0 & \text{if Re} = 0 \\ \frac{16}{Re} & \text{if Re} < 2100 \\ 0.079Re^{-0.25} & \text{if Re} \geqslant 2100 \end{cases} \quad (11)$$

The combination of two-phase multiplier and single-phase friction factor gives the following equation for the friction force:

$$F_\tau = \frac{1}{2}\Phi_l^2 C_f \pi d \rho_l (L_t - x)u^2 + \frac{1}{2}\sum \zeta \rho_l u^2 A \quad (12)$$

where the first part represents the viscous friction force and the second part the summation of all the different small friction losses (ζ) (e.g. T-section, valves).

Ultimately, the position of the meniscus can be determined as:

$$u = \frac{dx}{dt} \quad (13)$$

2.3. Conservation of energy

The final time-dependent equation of the numerical model describes the energy balance of the vapour bubble. The vapour temperature of the bubble is given by:

$$\frac{dT_v}{dt} = \frac{1}{m_v c_{vv}}(\dot{m}_v R_v T_v + \dot{Q}_{sens} - p_v A u) \quad (14)$$

$$\dot{Q}_{sens} = U_{sens}\pi d L_{dry}(T_e - T_v) \quad (15)$$

where c_{vv} is the vapour specific heat at constant volume assumed to be independent of the temperature and R_v is the specific gas constant. The heat exchange from evaporation and condensation is represented by the first term. The second term represents the sensible heat exchange of the tube wall with the vapour in the evaporator. The sensible heat exchange is given by Eq. (15) and is less than the evaporation and condensation heat exchange. The last term corresponds to the mechanical work. The pressure of the vapour bubble is determined using the ideal gas law. According to Rao et al. [1] and Gully et al. [10] this is a justified approximation because the vapour is superheated during the entire period of oscillation. The vapour pressure is modelled as:

$$p_v = \frac{m_v R_v T_v}{Ax} \quad (16)$$

3. Experimental investigation

3.1. Pump dimensions

The experimental setup is presented in Fig. 2. The orientation of the pump is vertical with respect to gravity to promote plug/slug flow and avoid the separations of liquid and vapour. The meniscus needs to encircle the entire tube wall to establish a pressure head. The vertical orientation slightly effects the meniscus stroke and the amount of output mass flow due to the gravitational force acting on the liquid and vapour. This effect can be neglected because of the low mass of the liquid and vapour.

According to a sensitivity analysis performed using the numerical model, the tube diameter is the most sensitive parameter regarding the output mass flow. Also, according to the model the tube diameter is proportional to the output mass flow. However, the tube diameter is limited due to the balance of gravity and surface tension at the meniscus. The theoretical critical inner tube diameter is a definition of the Eötvös number [11]:

$$d_{crit} = 2\sqrt{\frac{\sigma}{g(\rho_l - \rho_v)}} \quad (17)$$

During all experiments demineralized water was used as the working fluid. The critical diameter of water at ambient boiling temperature is approximately 5 mm. In order to guarantee pump operation, the internal tube diameter used in the experiments was 4 mm. The experimental pump is entirely constructed from stainless steel Swagelok part, the tube wall thickness is 1 mm and the length of the other sections is listed in Table 1.

3.2. Experimental setup

The left side of Fig. 2 shows two reservoirs that together represent a self-leveling reservoir at the inlet of the pump. The fluid level in the reservoir is kept at a constant level, equal to the height of the output of the pump to prevent the fluid level from having any effect on the output mass flow. Following the pump inlet tube to the right, the first pressure sensor is located before the supply check valve (Swagelok, SS-CHS8MM-1/3). After the T-section to the right, the discharge check valve is situated followed by the second pressure sensor. The temperature of the pump is measured at six different locations, the temperatures of the fluid are measured at three points, at the inlet, T-fitting and outlet. The remaining three thermocouples measure the evaporator temperature and the inlet and outlet temperatures of the condenser coolant. All mounting points of the thermocouples and the entire evaporator are isolated using fiberglass insulation. The evaporator section is heated using a Thermocoax heater, coiled around and soldered onto the tube. The condenser coolant counterflows: the direction of the flow is opposite to the direction of the meniscus displacement as it enters the condenser. The coolant flows through a filter and flowmeter, before it enters the condenser. The inlet temperature of the coolant is controlled by a thermostatic bath and the inlet and outlet temperatures are both measured. Finally, the fluid passes through a needle valve and is collected and weighed in the output reservoir at the right of Fig. 2. All sensors are sampled at 100 Hz and the runtime was 3 min per setting.

4. Experimental results

Experimental results are discussed for three different experiments with various operating conditions, as shown in Table 2. The evaporator input power is increased within the specified range with steps of 20 W and the condenser temperature is increased by 15 °C per step. At less than 30 W of input power no stable oscillations were observed and above 130 W the pump would suffer from evaporator dry-out. Also, the condenser flow rates are listed. The pump is tested with two different condenser flow rates to investigate the influence of the condenser flow rate.

4.1. Baseline experiment

To determine the influence of the check valves on the performance of the pump, a baseline experiment was conducted. The T-section and the check valves are removed and replaced with an acrylic tube marked with barlines having an equal internal diameter. The meniscus motion is recorded by a camera at 50 fps (see Fig. 3) to analyze the influence of the input power and condenser temperature on the output mass flow, as shown in Fig. 4. The ideal output mass flow is calculated by:

$$\dot{m}_{output} = \frac{A\rho_l \sum positive\ displacement}{run\ time} \quad (18)$$

The output mass flow is approximately proportional to the input power, the higher the input power, the more vapour is produced, the larger the meniscus stroke becomes, resulting in a higher output mass flow. At constant input power, the output mass flow increases

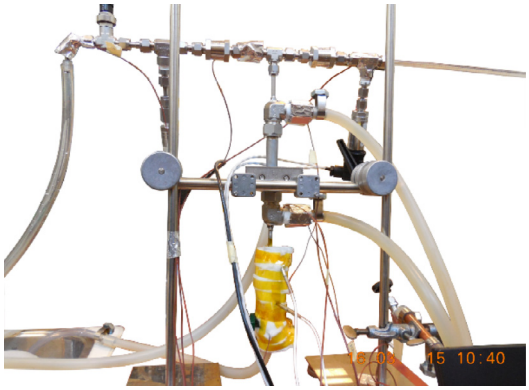

(a) photograph of the setup; vertically in the middle are the evaporator (insulated) on the bottom and the condenser (tube-in-tube) above.

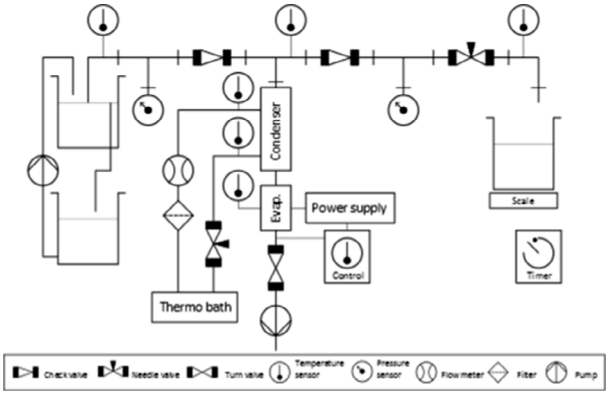

(b) schematic of the setup; on the left is a self-levelling supply reservoir, in the middle the pump tube and on the right the discharge valve with output reservoir.

Fig. 2. Experimental setup.

Table 1
Dimensions of the experimental pump.

Pump section	Unit
Length of the dead end (L_d)	20 mm
Length of the evaporator (L_e)	70 mm
Length of the adiabatic section (L_a)	35 mm
Length of the condenser (L_c)	150 mm

Table 2
List of conducted experiments with input parameters.

	Input power (W)	Condenser temp. (°C)	Condenser flow (L/s)
Video	30–130	15–45	0.02
1	30–130	15–45	0.02
2	30–130	15–45	0.004

with the increase in condenser temperature. This is likely caused by the fact that the fluid in the condenser cools down less, maintaining a higher temperature. When this fluid returns into the evaporator in the next cycle, the temperature difference with the saturation temperature is less, allowing for the earlier formation of a new vapour bubble. Also due to the higher condenser temperature, the vapour bubble progresses deeper into the condenser, which increases the meniscus stroke. Both mentioned assumptions are supported by the experimental results. Further, the oscillation shapes of the repetitive periods found in the base line experiment slightly differ from the described oscillation period of the section pumping principle and from experiments conducted by Rao et al. [1,2]. The observed oscillation period during the experiments showed one large displacement followed by a couple of smaller displacement (not properly shown in Fig. 3) instead of the one large followed by one small displacement.

4.2. Pump with check valves

Fig. 5 shows the influence of the input power and condenser temperature on the output mass flow of the pump with the T-section and check valves. Comparing the results of Figs. 4 and 5, two differences are noticeable. First, Fig. 5 shows that the increase in input power does not result in a higher output mass flow; a threshold value is observed in both plots. The pump has a maximum output mass of 0.0013 kg/s at an input power between 50 and 70 W. The average output mass flow is approximately 0.0010 kg/s. Second, any significant influence of the condenser temperature on the output mass flow is not observed during the pump experiments with the check valves. As is apparent, the baseline and pump experiments show significant differences in output mass flow. The mass flow is determined by the oscillation frequency and the pressure head generated by the pump. A higher pressure head increases the meniscus stroke and together with a higher oscillation frequency, will result in more output mass flow. To explain the differences in output mass flow, the frequencies and

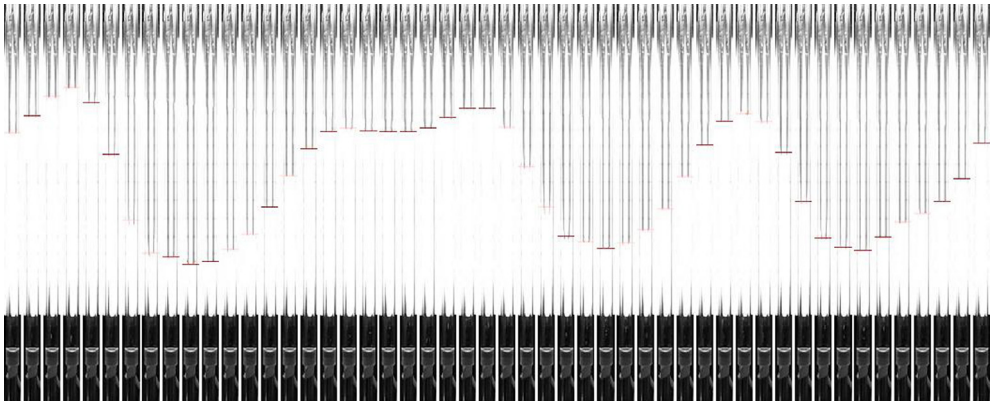

Fig. 3. 50 consecutive video frames (left to right) displaying the meniscus motion.

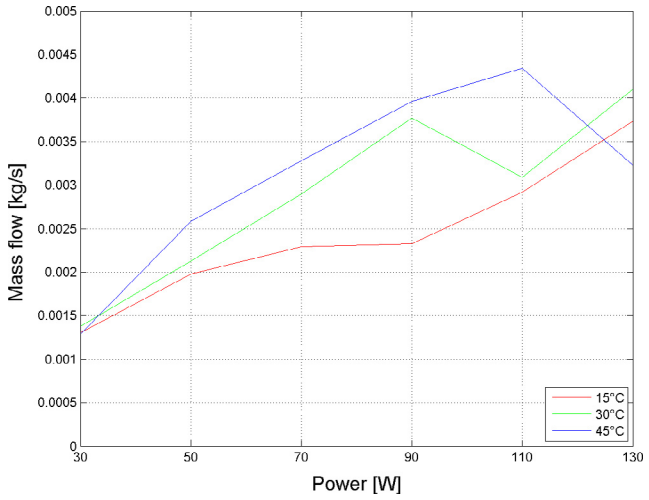

Fig. 4. Experimental results of video recording showing the input power vs. output mass flow. The decrease in output mass flow at higher input powers is caused by experimental limitations.

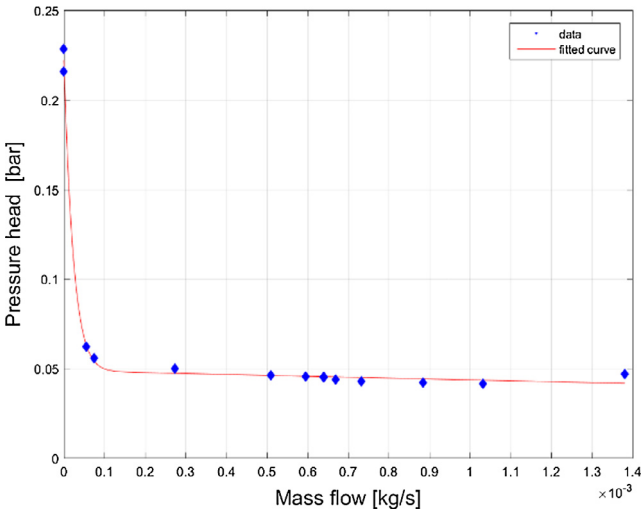

Fig. 6. Pump curve for an input power of 70 W.

pressure head of the pump with check valves and the baseline experiments are compared. The oscillation frequencies are determined using a FFT on the displacement signal from the video analysis and the pressure signal from the experimental pump. The pressure head of the pump with check valves is determined by taking the average of the top 10% of all pressure peaks. The pressure head of the baseline experiment is not measured but determined numerically.

The main frequency of the baseline experiment is generally less than the main frequency measured of the pump. The baseline experiment frequency plots show only one main frequency, always less than 8 Hz. In addition, the frequency plots of the pump show many frequencies above this 8 Hz and a much more chaotic signal. Fig. 6 also shows that the generated pressure head of the pump is less in comparison to the baseline experiment and does not increase when the power input is increased. The absence of pressure increase is inconsistent with the mentioned conclusion that at a higher input power more vapour is formed, thus increasing the pressure. This is likely due to the fact that during the pump experiments relatively cold fluid enters the pump each cycle. More energy is needed to heat this fluid to the saturation temperature leaving less energy for vaporization resulting in less pressure head and output mass flow. This theory is supported by the comparison of the output mass flow between the baseline experiment (Fig. 4) and the pump (Fig. 5). The difference in output mass flow between the two situations is larger for higher condenser temperatures. At higher condenser temperatures less energy is required for heating, leaving more energy for vaporization and oscillatory motion. The relatively cold fluid entering the pump during each cycle explains the absence of the condenser temperature influence in the pump experiment results. During the baseline experiment, the lowest temperature the fluid reaches is the set condenser temperature while during the pump experiments this temperature is more or less constant and equal to the temperature of the entering fluid. The entering temperature of the fluid for all experiments was around 21 °C; in most situations this was less than the condenser temperature.

The lower fluid temperature should also result in a lower average evaporator temperature for the pump in comparison to the baseline experiment. The average evaporator temperature for the pump experiments is higher for all settings. An explanation is given by the shorter meniscus stroke that does not reach as far into the evaporator section because part of the vapour bubble never condenses. A shorter meniscus stroke corresponds with the lower output mass flow and higher frequencies that were observed during the pump experiments.

4.3. Pump performance

The characteristics of a pump are described by the pump curve. For three settings, pump curves are experimentally determined by

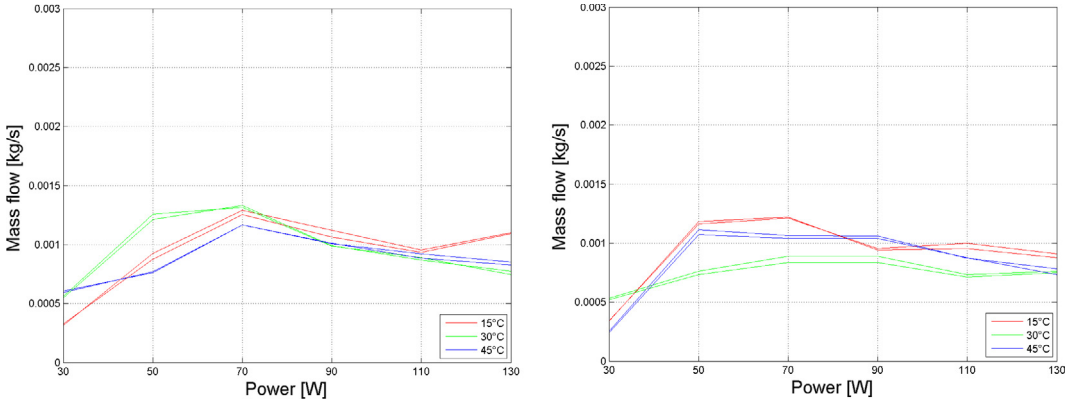

(a) condenser flow rate of 0.02 L/s (b) condenser flow rate of 0.04 L/s

Fig. 5. Experimental results of the pump with check valves showing the input power vs. output mass flow.

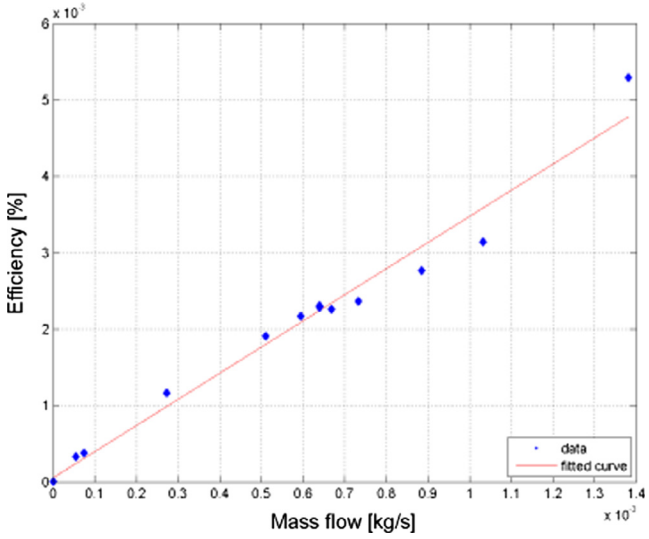

Fig. 7. Thermal pump efficiency vs. output mass flow for an input power of 70 W.

creating a stepwise back-pressure by partially closing the needle valve situated after the discharge check valve. The pressure head across the pump is the pressure difference between the two pressure sensors. The settings are: input powers of 50, 70 and 90 W, a condenser temperature of 15 °C and a condenser flow of 0.004 L/s. Fig. 6 shows the pump curve for the 70 W case. The other two settings produced approximately the same curve. The maximum pressure head delivered by the pump is approximately 0.25 bar for each of the settings, when the needle valve is fully closed. The pressure head rapidly decreases when the needle valve is opened. The rapid decrease in pressure is caused by the check valves. During the experiments it was observed that both check valves allow for some reverse flow. Probably due to the relatively high reseal pressure, and slow opening and closing responses, also reported by Dobson [3]. The slow response of the check valves may be caused by the inertia of the liquid acting as a damper.

4.4. Thermal and mechanical pump efficiency

The thermal pump efficiency indicates the extent to which the energy added by heat, is converted to output mass flow. The thermal pump efficiency is given by:

$$\eta_{thermal} = \frac{\frac{\dot{m}_{output}}{\rho_l}\Delta p}{\dot{Q}_{in}} \tag{19}$$

Thermal efficiency of the pump is calculated using the same parameter settings as used for the determination of the pump curve. A linear relation between the thermal pump efficiency and the output mass flow is observed, as shown in Fig. 7. The experimentally determined efficiency is in the order of 0.0037–0.0059%. This is about a factor 100 better than the only reported reference, namely the OOHPWP of Dobson which had an efficiency of 0.00003% [3]. The seemingly low efficiency is explained by observing the energy balance. The energy balance shows that around 5% of the input power is used for the evaporation of the water; the driving force behind the pump. The major part of the input power is used to reheat the new working fluid entering the pump to the saturation temperature.The mechanical pump efficiency indicates how well the experimental pump is operating in relation to the ideal situation. The mechanical pump efficiency is determined by:

$$\eta_{mechanical} = \frac{\dot{m}_{pump}}{\dot{m}_{ideal}} \tag{20}$$

For the ideal situation, the output mass flow of the baseline experiment is used as this indicates the ideal circumstances without any flow disturbance and resistance of the T-section and check valves. The mechanical pump efficiency are 46.7, 56.4 and 48.2% for the 50, 70 and 90 W cases, respectively. Approximately half of the upward meniscus stroke is converted into output mass flow. This substantiates the described losses due to fluid flow against the desired flow direction caused by the functioning of the check valves as described in the pumping principle.

4.5. Comparison to the numerical model

The validity of the numerical model is verified using the results obtained by the video baseline experiments, since the check valves, and therefore their influence, are not included in the model. As mentioned, the oscillation period in the baseline experiments was different than to be expected from other research studies [1,2]. The addition of the time-dependent liquid film thickness ensures that an oscillation period with one large displacement followed by a couple of smaller displacements can be captured by the numerical model, see Fig 8. This addition is in agreement with the findings of Rao et al. [1], in which they showed that the mass transfer rate from the liquid plug to the vapour bubble is a function of the triple-line and the liquid film thickness.

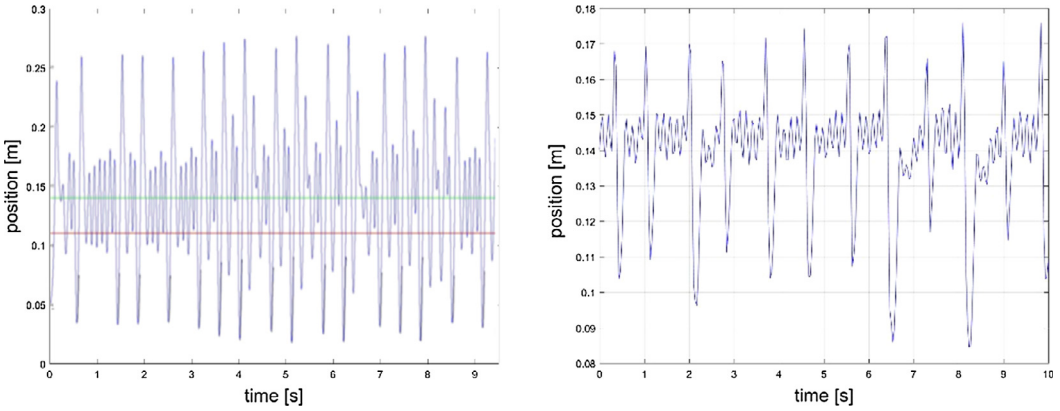

(a) oscillation profile numerical model

(b) oscillation profile baseline experiment

Fig. 8. Comparison between the numerical model and the baseline experiment.

Fig. 8 shows that the numerical model is able to capture approximately the same oscillation period as was observed in the experiments. This was however only valid for a number of the experimental settings. The oscillation frequency is higher and the amplitude of the displacement of the vapour bubble is larger in the numerical model than in the experiments. The model functioned stable when for instance pentane, also used by Rao et al. [1–2], was used as a working fluid. However, for water as a working fluid the numerical model was unstable and not able to prescribe the oscillation motion for most of the settings. The unstable performance of the model is likely caused by the high vapour-liquid density ratio of water in comparison to pentane. The numerical model is more sensitive to small changes in input power, heat transfer coefficients and the initial liquid film thickness.

5. Conclusions

A first baseline experiment showed a proportional relation between the input power and the output mass flow. The output mass flow increased when the condenser temperature was increased. The experiments conducted with the pump with check valves gave different results. During all experiments, the measured output mass flow was a factor 2–3 less than that of the baseline experiment. The pump experiments showed that the increase of the evaporator input power did not result in more output mass flow and a threshold value was observed. The pump worked best, based on the efficiency between input power and output mass flow, for input powers between 50 and 70 W.

Any significant influence of the condenser temperature on the output mass flow was not observed during the experiments with the pump, due to the fact that relatively cold working fluid enters the tube during each cycle. Therefore, more energy is needed to heat this fluid to the saturation temperature leaving less energy for vaporization. This results in less vapour generation, a lower pressure head and less output mass flow. Because less vapour is generated per unit of time, the stroke of the meniscus decreases as well. This is reflected by the frequency analysis showing a slightly higher oscillation frequency for the pump in comparison to the baseline experiment. The oscillation frequency of the prototypes is between 5 and 7 Hz.

The pump curves show a maximum pressure head of 0.25 bar while operating at an ambient pressure. The average output mass flow is approximately 0.0010 kg/s. Finally, the thermal efficiency of the prototype pump is in the order of 0.0037–0.0059% and the mechanical efficiency is around 50%.

Acknowledgement

The authors would like to thank Dr. Aswin Pauw of the Netherlands Aerospace Centre (NLR) for his contributions and assistance during the experiments.

Appendix A. Supplementary material

Supplementary data associated with this article can be found, in the online version, at http://dx.doi.org/10.1016/j.applthermaleng.2017.02.063.

References

[1] M. Rao, F. Lefèvre, S. Khandekar, J. Bonjour, Heat and mass transfer mechanisms of a self-sustained thermally driven oscillating liquid-vapour meniscus, Int. J. Heat Mass Transf. 86 (2015) 519–530.
[2] M. Rao, F. Lefèvre, S. Khandekar, J. Bonjour, Understanding transport mechanism of a self-sustained thermally driven oscillating two-phase system in a capillary tube, Int. J. Heat Mass Transf. 65 (2013) 451–459.
[3] R.T. Dobson, An open oscillatory heat pipe water pump, Appl. Therm. Eng. 25 (4) (2005) 603–621.
[4] S.P. Das, V.S. Nikolayev, F. Lefevre, B. Pottier, S. Khandekar, J. Bonjour, Thermally induced two-phase oscillating flow inside a capillary tube, Int. J. Heat Mass Transf. 53 (19–20) (2010) 3905–3913.
[5] R.T. Dobson, Theoretical and experimental modelling of an open oscillatory heat pipe including gravity, Int. J. Therm. Sci. 43 (2) (2004) 113–119.
[6] M. Rao, F. Lefevre, J. Bonjour, Thermally induced two-phase oscillating flow inside a capillary tube, in: 16th International Heat Pipe Conference, Lyon, France, 2012.
[7] Y. Han, N. Shikazono, The effect of bubble acceleration on the liquid film thickness in micro tubes, Int. J. Heat Fluid Flow 31 (4) (2010) 630–639.
[8] D. Chisholm, A theoretical basis for the Lockhart-Martinelli correlation for two-phase flow, Int. J. Heat Mass Transf. 10 (12) (1967) 1767–1778.
[9] R.W.M. Lockhart, R.C. Martinelli, Proposed correlation of data for isothermal two-phase, two-component flow in pipes, Chem. Eng. Prog. 45 (1949) 39–48.
[10] P. Gully, F. Bonnet, V.S. Nikolayev, N. Luchier, T.Q. Tran, Evaluation of the vapour thermodynamic state in PHP, in: Proc. 17th International Heat Pipe Conference, Kanpur, India, 2013.
[11] S. Khandekar, N. Dollinger, M. Groll, Understanding operational regimes of closed loop pulsating heat pipes: an experimental study, Appl. Therm. Eng. 23 (6) (2003) 707–719.